http://dx.doi.org/10.5935/0103-5053.20150028

J. Braz. Chem. Soc., Vol. 26, No. 4, 695-704, 2015.
Printed in Brazil - ©2015 Sociedade Brasileira de Química
0103 - 5053 $6.00+0.00

Article

CO Oxidation Catalyzed by Ag Nanoparticles Supported on SnO/CeO_2

Inayat A. Khan,[a] Nida Sajid,[a] Amin Badshah,*[a] Muhammad H. S. Wattoo,[a] Dalaver H. Anjum[b] and Muhammad A. Nadeem[a]

[a]*Catalysis and Nanomaterial's Lab 27, Department of Chemistry, Quaid-i-Azam University, 45320 Islamabad, Pakistan*

[b]*Imaging and Characterization Lab, King Abdullah University of Science and Technology, Thuwal, Saudi Arabia*

Ag-Sn/CeO_2 catalysts were synthesized by the co-precipitation method with different Ag-Sn wt.% loadings and were tested for the oxidation of CO. The catalysts were characterized by powder X-ray diffractometry (XRD), scanning electron microscopy (SEM), high-resolution transmission electron microscopy (HRTEM), energy dispersive X-ray spectroscopy (EDS), and selected area electron diffraction (SAED) techniques. UV-Vis measurements were carried out to elucidate the ionic states of the silver particles, and the temperature-programmed reduction (TPR) technique was employed to check the reduction temperature of the catalyst supported on CeO_2. There are peaks for silver crystallites in the X-ray diffraction patterns and the presence of SnO was not well evidenced by the XRD technique due to sintering inside the 3D array channels of CeO_2 during the calcination process. The Ag-Sn/CeO_2 (4%) catalyst was the most efficient and exhibited 100% CO oxidation at 100 °C due to small particle size and strong electronic interaction with the SnO/CeO_2 support.

Keywords: co-precipitation, crystallites, energy dispersive X-ray spectroscopy, reducibility

Introduction

Silver oxide nanoparticles (NPs) are considered excellent catalysts for many catalytic reactions such as formaldehyde synthesis, NO_x abatement, ethylene epoxidation, oxidative coupling of methane, selective oxidation of ammonia and ethylene glycol, partial oxidation of benzyl alcohol and oxidation of styrene and carbon monoxide.[1-17] The catalytic performance of silver NPs largely depends on surface area, surface texture, synthetic methods and reaction conditions. It has been reported by researchers that pretreatment of silver oxide in O_2 at high temperature results in the formation of subsurface oxygen which activates the catalyst.[18-23] There are endorsements that Ag^0 species is an excellent catalyst below 140 °C, while above 140 °C, Ag^+ is much active for CO oxidation.[5] CO catalytic oxidation has been extensively studied for its widespread applications in the subject of environmental protection, closed cycle CO laser and selective oxidation of CO in reformer gases for fuel cell applications, etc.[24-26] A number of metal nanocatalysts (e.g., Au/TiO_2, Pt/Al_2O_3, etc.) have been recognized to be very effective in CO oxidation reaction.[27-29] It has been accepted that silver dispersed on silica is more dynamic and stable than silver supported on carbon nanotubes or reducible oxides (Mn_2O_3, TiO_2).[30-32] Afanasev *et al*.[33] have reported that Ag supported on fumed silica (4 wt.%) is very effective in CO oxidation reaction [T_{100} = 30 °C]. On the other hand, Yu *et al*.[34] testified that the catalytic efficiency of silver NPs supported on SiO_2 for CO oxidation at ambient temperature is quite low due to particle agglomeration and single phase of the support materials. Zhang *et al*.[35] have also reported that silver NPs on mesoporous silica (SBA-15) is an ideal candidate for CO oxidation (T_{98} = 20 °C) and they have proposed evaporation-deposition-diffusion mechanism for metal-supported interactions. Zhu *et al*.[36] have published that gold NPs confined within the mesoporous silica are stable after heat treatment. Sun *et al*.[37] explored that due to the confinement effect of mesoporous channels of the support for silver NPs, the particles are located outside as well as inside the channels even after thermal treatment at high temperature (500 °C).

The surface defects, morphology and re-crystallization of solids play an important role in the surface reaction of

*e-mail: aminbadshah@yahoo.com

gases, gas diffusion and adsorption.[38-40] The unsaturated bonds present on the surface of solid hybrid/composite materials act as active sites for gas adsorption. The changes in morphology may be thermal or reaction induced.[39] The thermally induced morphological changes occur with or without the presence of reacting atmosphere while reaction induced morphological change takes place only in a reacting atmosphere. These induced changes result in a structure different from those formed even after thermal treatment in inert atmosphere or vacuum.[39,41-43] This phenomenon is called adsorbate-induced alterations of the surface free energy. The adsorption of O_2 on solids at elevated temperature decreases the surface free energy. However, the thermal treatment of silver at high temperature is not affordable due to low melting point (960 °C), reversible redox behavior, sintering inside the support channels and morphological changes.[17] Thus, there is a need of third body metal to facilitate the redox behavior of silver and also its sintering inside the support channels without severe thermal treatment.

In the present work, Ag-Sn (with equal wt.% loading) bimetallic nanocatalysts supported on ceria were synthesized for CO oxidation reaction using co-precipitation method. It was observed that the tin oxide sintered in the 3D array of ceria during thermal treatment (at 400 °C) formed a platform for silver NPs. The tin oxide particles facilitated the silver sintering and controlled its redox behavior for catalytic purposes.[44-46] Our research group is still interested to further investigate and propose a mechanism for this dual function of tin oxide NPs in catalysis.

Experimental

Synthesis of ceria and catalysts

For the synthesis of ceria, $Ce(NO_3)_3 \cdot 6H_2O$ (1.5 g; 3.45 mmol) was dissolved in 25 mL of distilled water. To the cerium salt solution, aqueous NaOH (2 mol L^{-1}; pH > 12) was added dropwise under magnetic stirring at room temperature leading to the formation of a yellow precipitate. The product was obtained at folded filter paper, washed with excess distilled water and dried at 105 °C.[47]

$$Ce^{3+} + H_2O \rightarrow Ce(OH)^{3+} + H^+ + e^- \quad \text{(oxidation at pH > 10)} \quad (1)$$

$$Ce(OH)^{3+} + 3OH^- \rightarrow Ce(OH)_4 \text{ (hydrolysis)} \quad (2)$$

$$Ce(OH)_4 \rightarrow CeO_2 \cdot 2H_2O \quad (3)$$

$$CeO_2 \cdot 2H_2O \rightarrow CeO_2 + 2H_2O \text{ (drying at 105 °C)} \quad (4)$$

Similarly, co-precipitation method was employed for the synthesis of $Ag\text{-}Sn/CeO_2$ catalysts for which CeO_2 slurry was prepared in distilled water (25 mL) and the salt solutions ($AgNO_3$ and $SnCl_2 \cdot 2H_2O$) with an appropriate quantity for the catalysts were added dropwise. The salt solutions were added separately to avoid the precipitation of Ag^+ and Cl^- ($Ag^+ + Cl^- \rightarrow AgCl_{ppt}$). pH of the mixture was maintained at 12 by adding NaOH solution dropwise under gentle stirring at room temperature. Powdered catalysts were obtained after washing with distilled water till the pH came to neutral. After drying, the catalysts were thermally treated at 400 °C to remove impurities. The different catalysts were synthesized like $Ag\text{-}Sn/CeO_2$ (1%), $Ag\text{-}Sn/CeO_2$ (2%), $Ag\text{-}Sn/CeO_2$ (3%) and $Ag\text{-}Sn/CeO_2$ (4%) in accordance with the successive increase in the Ag-Sn wt.% loadings.

$$Ag^+ + H_2O \rightarrow Ag(H_2O)^+ \quad (5)$$

$$2Ag(H_2O)^+ + 2OH^- \rightarrow Ag_2O + 3H_2O \quad (6)$$

$$Ag_2O + H_2O \rightarrow 2Ag + 2OH^- \quad (7)$$

$$Sn^{2+} + 2OH^- \rightarrow Sn(OH)_2 \quad (8)$$

$$Sn(OH)_2 \rightarrow SnO \cdot H_2O \quad (9)$$

$$SnO \cdot H_2O \rightarrow SnO + H_2O \quad (10)$$

Characterization techniques

PANalytical diffractometer (X'Pert PRO 3040/60) with a Cu K_α (λ = 1.544206 Å) radiation generated at 40 kV and 30 mA was used for X-ray diffractometry (XRD) measurements, which were carried out at a speed of 0.015 degree s^{-1}. Surface morphology of catalysts was examined by scanning electron microscopy (SEM) (JEOL JSM-6610LV) and high-resolution transmission electron microscopy (HRTEM) of samples was conducted with FEI Company Titan 80-300 CT TEM by operating it with the acceleration voltage of 300 kV. Moreover, the energy dispersive X-ray spectra (EDS) of samples were also acquired during their conventional transmission electron microscopic (CTEM) investigations. Finally the selected area electron diffraction (SAED) patterns from various regions of samples were acquired for the determination of crystal structures. It should be noted that the entire electron micrographs acquired with TEM were recorded on a 4 k × 4 k charge coupled device (CCD) camera of model US4000 from Gatan, Inc. The UV-Visible (diffuse reflectance) spectra were recorded with a UV-1800 spectrophotometer (Shimadzu). The temperature-programmed reduction (TPR) analyses of the samples were carried out on a Micromeritics (Chemisorb-2750) with H_2/Ar (10 vol.%) as a reducing agent (flow rate of 35 cm^3 min^{-1}) at a heating rate of 15 °C min^{-1} from room temperature to 800 °C. Hydrogen consumption was measured by thermal conductivity detector (TCD). Prior

to the reduction, the samples (120 mg) were pretreated in helium at 300 °C for 90 min.

CO oxidation experiments

The CO oxidation catalytic activity was conducted by a fixed bed flow reactor system with a quartz tube (5 mm outer diameter) fixed in a tube furnace (Nabertherm B 180) at atmospheric pressure and 0.3 g of catalyst load. The reactant gas, consisting of CO, O_2 (1:2 vol.%) and balanced with Ar, was supplied with mass flow controller and mixed with each other, and then the final reactant gas mixture (35 cm^3 min^{-1}) was passed through the catalyst bed. The samples were activated at 350 °C for 120 min by Ar flow (35 cm^3 min^{-1}) before the reaction. The CO oxidation reaction was studied in the temperature range of 25-250 °C and the reactor effluent was analyzed using an online gas chromatograph system (GC-2010 Plus, Shimadzu) with Molecular Sieves 5A (30 m) column and TCD. Conversion of CO to CO_2 was calculated from the gas chromatographic (GC) data according to the equation: $X_{co} = [CO]^* - [CO] / [CO]^*$; where X_{co} is CO conversion, [CO]* and [CO] are the inlet and outlet gas concentrations (ppm), respectively.

Results and Discussion

Characterization of the catalysts

Powder X-ray diffractometry (PXRD) technique was used to investigate the chemical composition and crystalline phases of the synthesized catalysts. The X-ray diffraction pattern of the free support (CeO_2) and catalysts with different Ag-Sn wt.% loading is presented in Figure 1 after calcination at 400 °C. There are peaks in the diffraction pattern a (Figure 1) at 2θ = 28.6, 47.3, 56.4, and 72.4° corresponding to the (111), (220), (311) and (400) lattice planes, respectively, (Joint Committee on Powder Diffraction Standards (JCPDS) cards file No. 00-004-0593) of CeO_2. The X-ray pattern shows the three-dimensional cubic structure of CeO_2 with Fm-3m space group. The calculated crystallite size from the respective 2θ values falls in the range of 4.6-10 nm and the average size is 7 nm. It is also obvious from the diffraction pattern of CeO_2 that all the characteristic peaks are broad and of quite low intensity due to small particle size. In catalysis, small particle size of the support plays an important role in metal particles distribution and reaction selectivity like CO oxidation. In the X-ray diffraction, patterns (Figure 1, patterns b, c, d and e) of the nanocatalyst peaks are present for CeO_2, SnO, Ag_2O and Ag. Ag characteristic peaks are present at 2θ = 44.4, 64.6 and 77.6° due to the (200), (220) and (311) lattice planes, respectively, in all the catalysts systems. Small peaks at 2θ = 54.3°, (Figure 1, patterns b and c), 69.2° (Figure 1, pattern d) and 82.4° (Figure 1, patterns d and e) correspond to the (220), (222) and (400) lattice planes, respectively, of Ag_2O in the synthesized catalysts. Peak at 2θ = 38.4° corresponds to the (111) lattice plane of Ag and (200) lattice plane of Ag_2O. The observed mirror indices for Ag and Ag_2O reflect cubic (fcc) geometry (JCPDS cards file No. 00-001-1164 for Ag and 00-001-1041 for Ag_2O) with space groups Fm-3m and Pm-3m, respectively. Peak at 2θ = 33.4° corresponds to the (002) lattice plane of CeO_2 and to the (111) lattice plane of Ag_2O and this peak can also be assigned to SnO (JCPDS cards file No. 00-001-0902) in all the catalyst diffraction patterns. Other corresponding peaks of SnO do not appear in the diffraction pattern of the catalysts probably due to two possible reasons: (*i*) the particle size is very small, i.e., below the detection limit of X-ray radiation; and (*ii*) SnO is intermingled in the 3D array of cerium(IV) oxide in such a way that it forms a combined plate form for silver NPs and is not explored in the XRD analysis. Peaks responsible for Ag and Ag_2O crystallites become intense and sharper in the XRD pattern of Ag-Sn/CeO_2 (3%) catalyst system (Figure 1, pattern d), suggesting comparatively large particle size. It is clear from Figure 1 that the diffraction peaks for Ag and Ag_2O are not of equal intensity suggesting that the crystallites are not of equal size. The crystallite size (d) calculated for Ag and Ag_2O at 2θ = 77.6 and 38.4° using the Scherrer equation is given in Table 1. There is no linear relationship between particle size and Ag-Sn wt.% loading. Possible reason for this nonlinear relationship is the phenomenon of particle agglomeration that takes place during co-precipitation synthesis. In case of Ag-Sn/CeO_2 (3%), the particle size of Ag and Ag_2O reaches up to 18.32 and 22.12 nm (Table 1), respectively, showing maximum crystallite aggregates formation. The calculated crystallite size (d) at 2θ = 33.5° for SnO via Scherrer equation ranges from 2 to 4 nm in all the catalysts systems.

An EDS spectrum of Ag-Sn/CeO_2 (4%) catalyst acquired in CTEM mode is shown in Figure 2, which ratifies peaks for oxygen, silver, tin and cerium. There is a single point at 3 keV for silver, two peaks at 3.4 and 3.55 keV for tin and two peaks at about 3.9 and 5.2 keV for cerium metal. Peaks are originated at 8 and 0.35 keV due to copper grid and carbon polish, used for sample analysis. The EDS analysis illustrates that tin is the part of catalyst system but its presence is not confirmed by PXRD technique.

For surface morphology investigation, SEM analysis was carried out and the images are presented in Figures 3a-d. The SEM images clearly show the three dimensional cubic morphology of the CeO_2 supported nanocatalysts. HRTEM

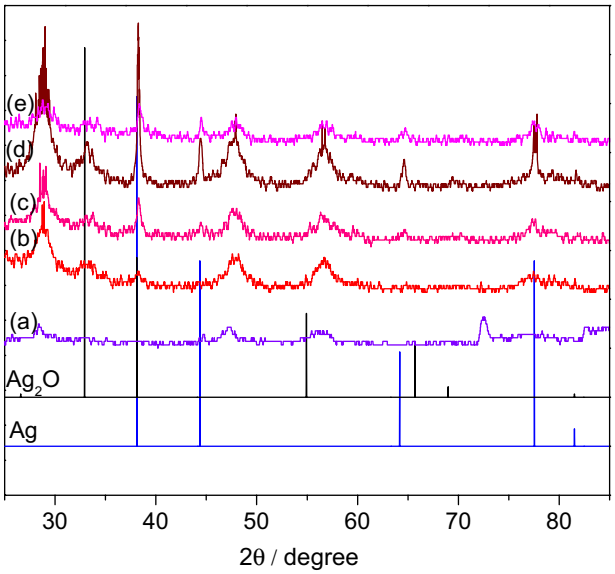

Figure 1. XRD pattern of: (a) CeO_2 support; (b) (Ag-Sn/CeO_2) (1%); (c) (Ag-Sn/CeO_2) (2%); (d) (Ag-Sn/CeO_2) (3%); and (e) (Ag-Sn/CeO_2) (4%). Cu Kα (λ = 1.544206 Å) X-ray radiation source generated at 40 kV and 30 mA was used for XRD analysis.

Table 1. Ag/Ag_2O crystallite size from powder XRD at 2θ = 77.6 and 38.4°, mean particle size of catalysts from TEM analysis

Catalyst	Particle size / nm		
	XRD		TEM
	Ag	Ag_2O	
Ag-Sn/CeO_2 (1%)	6.08	6.66	5.50 ± 1.907
Ag-Sn/CeO_2 (2%)	6.19	23.62	4.67 ± 1.773
Ag-Sn/CeO_2 (3%)	18.32	22.12	7.55 ± 1.21
Ag-Sn/CeO_2 (4%)	2.74	5.52	3.67 ± 1.936

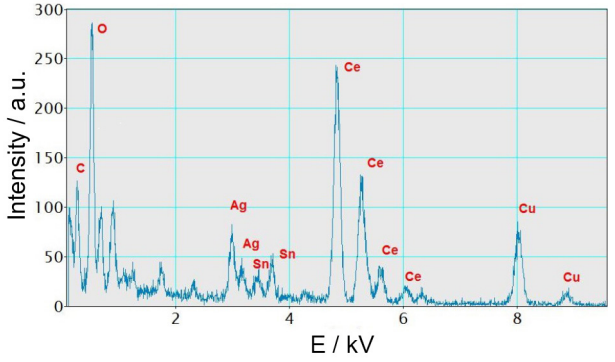

Figure 2. Representative EDS spectrum of Ag-Sn/CeO_2 (4%) catalyst shows Ag, Sn and Ce as the main constituents of catalyst's combination. The EDS spectrum of sample was acquired during their TEM investigation.

and SAED techniques were employed to investigate the size and distribution of nanoparticles supported on CeO_2. The results compiled by these techniques are presented in Figures 4a-d, which illustrate that the silver-tin particles are well dispersed on ceria matrix with narrow size distribution and small average particle size (3-8 nm) (Figure 5) after calcination in air at 400 °C. It has been reported by Zhang *et al.*[17] that when the catalysts are treated at 500 °C temperature in O_2 silver's particles, dispersion increases but no such changes have been observed in this case which may be due to the stability of the silver NPs in the presence of tin oxide providing synergistically a platform along with ceria. No clear distinction can be drawn between silver and tin particles in the HRTEM micrographs due to a small difference in their atomic numbers. Collectively the particle size of the Ag-Sn in 4 and 2% metal loading catalysts is small in comparison to 3 and 1% metal loading catalysts (Table 1 and Figure 5). So, no clear correlation with increasing metal loading and particle size is observed in this study. SAED results are in good agreement with PXRD patterns of the catalysts.

The ionic states of silver in Ag-Sn/CeO_2 catalysts were further studied by UV-Vis measurements after thermal treatment at 400 °C in air. Figure 6 is the UV-Vis spectra of Ag-Sn/CeO_2 catalysts with different Ag-Sn wt.% loading. Generally, there are three bands from different oxidation states of silver reported in different research articles. These are absorption bands at 220 nm for Ag^+, at 275 nm for $Ag_n^{\delta+}$ clusters and at 410 nm for metallic Ag^0 NPs.[17] In the work presented, in the absorption spectra of Ag-Sn/CeO_2 catalysts, no band is observed at 410 nm for Ag^0 in all catalysts combinations suggesting the non-interaction mode of Ag^0 with support because of the reduced form. There are two surface resonance plasmon centered at 310 and 350 nm in the catalysts having 1, 2, and 3 wt.% loading of metals while the catalyst with 4 wt.% metal loading has only a small band at 350 nm. The band, centered at 310 nm, is attributed to the transition of electron from $4d^{10}$ to $4d^9 5s^1$ of highly dispersed Ag^+ ions, while band centered at 350 nm is due to the $Ag_n^{\delta+}$ clusters. The observed red shift for Ag^+ (from 220 to 310 nm) and for $Ag_n^{\delta+}$ (from 275 to 350 nm) in case of Ag-Sn/CeO_2 (3%), Ag-Sn/CeO_2 (2%), and Ag-Sn/CeO_2 (1%) catalysts is due to the strong interaction of silver particles with SnO/CeO_2 support, which synergistically facilitates the electronic transition.[1] In UV-Vis measurements the intensity of the band is related to the average size of the NPs. When the particles aggregate and particle size increases comparatively (up to certain extent), the intensity of the absorption band increases as in the case of Ag-Sn/CeO_2 (3%) catalyst while band of 310 nm for Ag^+ disappeared in Ag-Sn/CeO_2 (4%) catalyst combination, which is due to small particle size as confirmed by HRTEM and PXRD analysis. In the UV-Vis spectrum of pure CeO_2 support, there is a broad absorption band, centered at 370 nm for localized oxygen-cerium charge transfer transition.[48] The CeO_2 characteristic band in the different catalysts combination does not appear at the

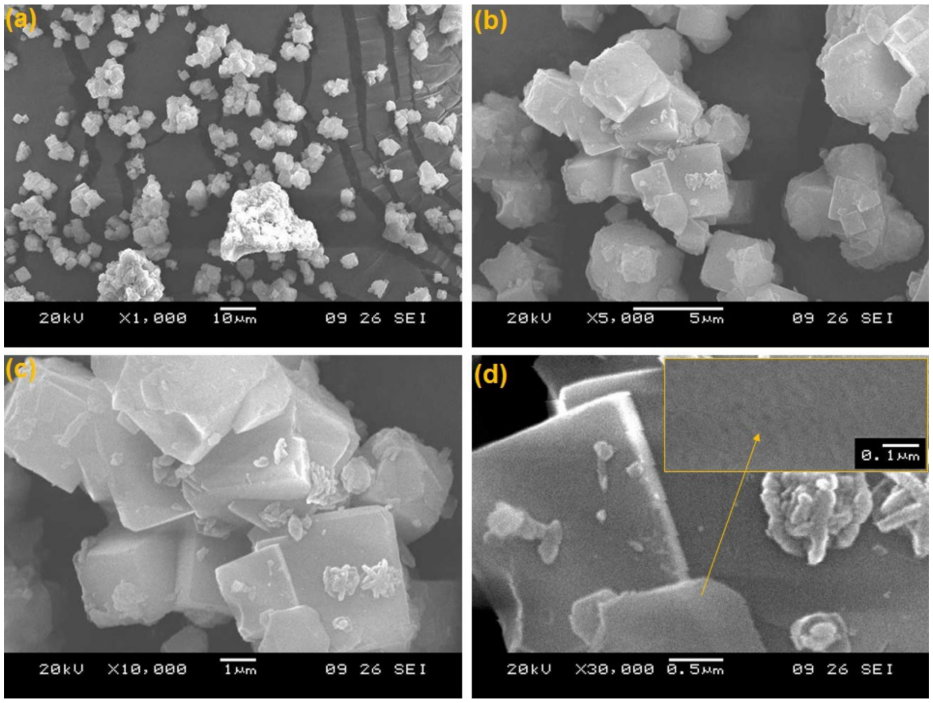

Figure 3. SEM images showing the cubic morphology (a, b, c and d) and porous plane (inset of image d) of the Ag-Sn/CeO_2 nanocatalysts.

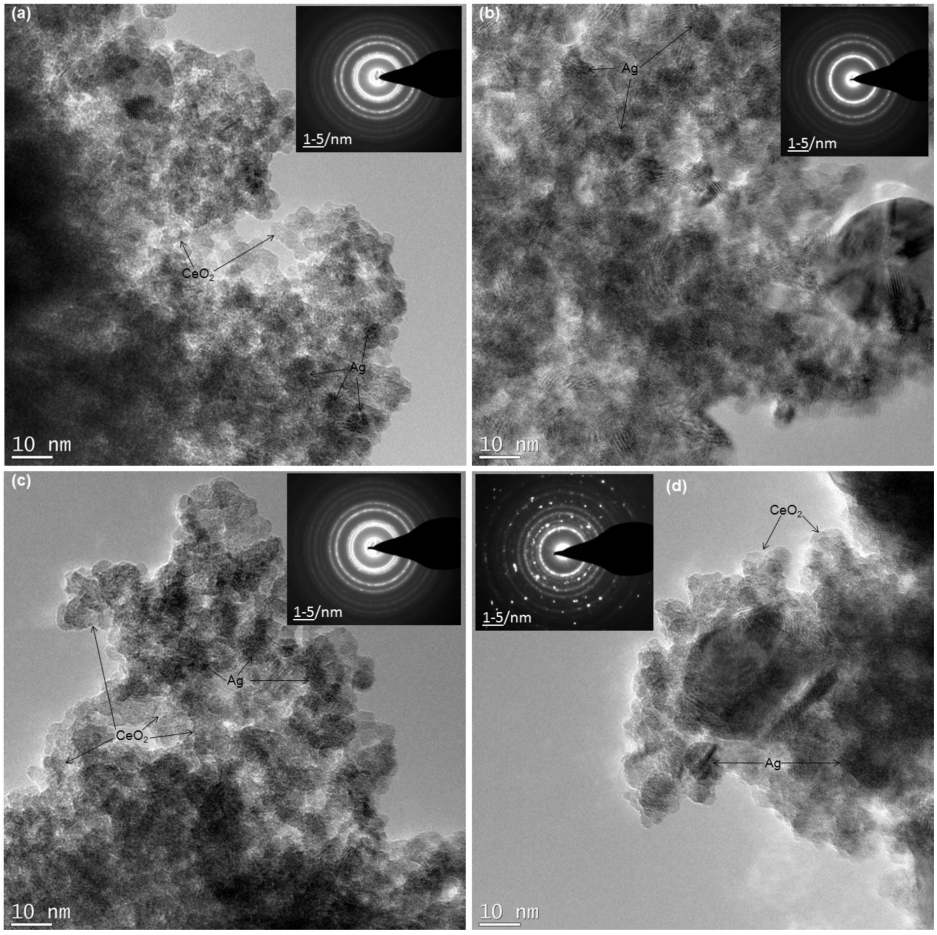

Figure 4. HRTEM images for: (a) Ag-Sn/CeO_2 (4%); (b) Ag-Sn/CeO_2 (1%); (c) Ag-Sn/CeO_2 (3%); and (d) Ag-Sn/CeO_2 (2%) catalysts. The inset pictures are the SAED pattern of the respective catalyst. The HRTEM analysis was carried out with an acceleration voltage of 300 kV.

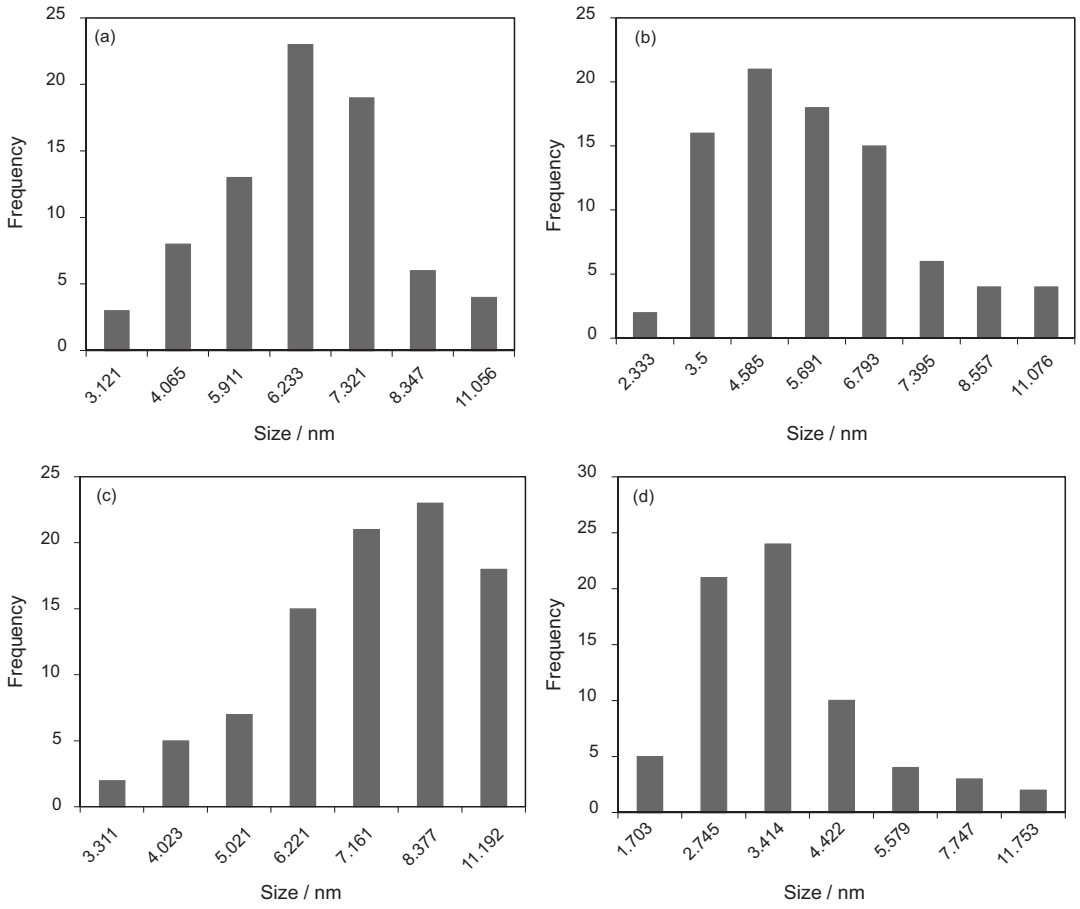

Figure 5. Particle size distribution from TEM analysis of CeO_2 supported nanocatalysts: (a) 1%; (b) 2%; (c) 3%; and (d) 4%.

respective λ_{max} probably due to the electronic interaction between the metal load and support. The absence of CeO_2 absorption band distinctly in the catalyst systems further confirm the red shift for Ag^+ and $Ag_n^{\delta+}$ clusters and blue shift for CeO_2 due to silver support (SnO/CeO_2) interaction.[49] The UV-Vis studies strongly suggest the interaction of silver ionic species with SnO/CeO_2 which affects its redox properties during catalysis. The primary focus of this work is to control the redox property of silver without harsh thermal treatment by incorporating a third body metal, which is conclusively shown by UV-Vis studies.

The reducibility of the synthesized catalysts was examined by TPR technique and the H_2-TPR profiles are presented in Figure 7. In the examined temperature range (25-800 °C) the catalyst's H_2-TPR profiles consist of three reduction zones, which are in the temperature range of 50-280 °C (α), 280-430 °C (β) and 430-750 °C (γ), respectively. According to the reported literature work, there is no reduction peak below 400 °C for pure support (ceria).[50] In our studies several reduction peaks are present in the H_2-TPR profiles of the $Ag\text{-}Sn/CeO_2$ catalysts in the whole temperature range. Peaks in the temperature range of 50-280 °C (α-temperature zone) can be assigned to the

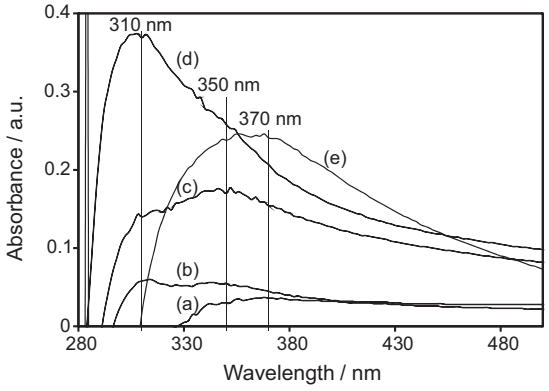

Figure 6. UV-Vis absorption spectra of: (a) $Ag\text{-}Sn/CeO_2$ (4%); (b) $Ag\text{-}Sn/CeO_2$ (1%); (c) $Ag\text{-}Sn/CeO_2$ (2%); (d) $Ag\text{-}Sn/CeO_2$ (3%); and (e) CeO_2.

reduction of oxygen adsorbed on the surface of catalyst and to the reduction of Ag_2O to Ag.[51] In the total amount of silver, the oxidized species (Ag_2O) is not of equal amount; so, the peak responsible for Ag^+ reduction is not of equal intensity in all the catalyst combinations. Consequently, the peak area for Ag^+ reduction, i.e., the amount of consumed hydrogen does not increase gradually with increasing amount of silver loading. Peaks in the β-temperature zone (280-430 °C) of the four catalysts are due to the

reduction of surface capping oxygen of SnO.[44] There is an intense peak and a small shoulder in the γ-temperature zone (430-750 °C) in the H_2-TPR profiles of Ag-Sn/CeO_2 (1%), Ag-Sn/CeO_2 (2%) and Ag-Sn/CeO_2 (3%) catalysts. The intense peak can be assigned to the reduction of bulk cerium(IV) oxide while the shoulder is due to the reduction of surface capping oxygen of ceria.[52] In the H_2-TPR profile of Ag-Sn/CeO_2 (4%) catalyst, there is a small peak and a shoulder with almost the same intensity in the γ-temperature zone for the reduction of bulk and surface capping oxygen of ceria. The decrease in peak intensity for ceria reduction in Ag-Sn/CeO_2 (4%) catalyst is probably due to the small particle size and high surface area of CeO_2, which ensures the dispersion of metals over the surface. The dispersion of metals over the support surface further facilitates the electronic interaction of metal with support and lower hydrogen consumption for CeO_2 reduction. Alternatively, it is obvious from the β-temperature zone that the peak responsible for the reduction of surface capping oxygen of SnO is comparatively intense in the H_2-TPR profile of Ag-Sn/CeO_2 (4%) catalyst, presenting high consumption of hydrogen because of their enhanced electronic interaction. Kharlamova *et al.*[49] have also reported that Ag_2O and CeO_2 interact with each other strongly and there is a simultaneous reduction of both in α-temperature zone. Therefore, the peak responsible for CeO_2 reduction in γ-temperature zone is very minute for Ag-Sn/CeO_2 (4%) catalyst in comparison with other options. There is shifting of peaks with changing metal wt.% loading on support due to interaction with support up to different extent. In the H_2-TPR profiles of Ag-Sn/CeO_2 (2%) and Ag-Sn/CeO_2 (3%) catalysts the reduction maxima for Ag^+ ion shift toward low temperature as compared to Ag-Sn/CeO_2 (1%) catalyst profile probably due to: (*i*) comparatively weak interaction of Ag^+ with support; and (*ii*) the increasing quantity of SnO also facilitates the

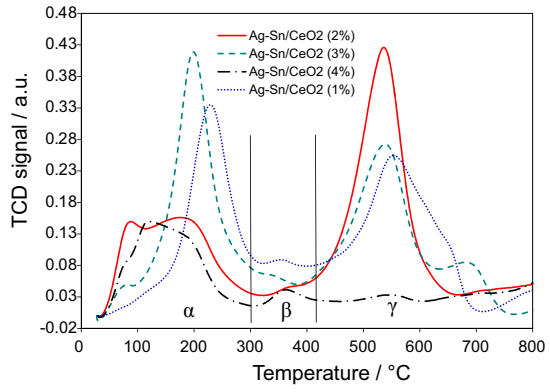

Figure 7. H_2-TPR profiles of CeO_2 supported nanocatalysts in the temperature range of 25 to 800 °C. The H_2-TPR of samples were carried out with H_2/Ar (10 vol.%) as a reducing agent (flow rate of 35 cm^3 min^{-1}) at a heating rate of 15 °C min^{-1}.

reducibility of Ag^+. The peak intensity in the TPR profile has a relationship with the size of nanocatalysts particle. The present TPR studies have shown that Ag-Sn/CeO_2 (4%) catalyst system consists of small reduction peaks due to very fine particle size of metals and support as well.

Catalytic activity

Catalytic activities of Ag-Sn/CeO_2 catalysts and pure support CeO_2 prepared by co-precipitation method and later calcination at 400 °C towards CO oxidation are shown in Figure 8. The CO conversion increases with reaction temperature and all the silver catalysts can completely oxidize CO to CO_2 at certain temperature. For 99% conversion of CO, the temperature for catalysts with 1, 2, 3, and 4% metal loading are 152, 133, 157, and 98 °C, respectively (Table 2). Meanwhile, pure support CeO_2 is also active in CO oxidation reaction and demonstrates 99% conversion at about 170 °C. The activity slope of CeO_2 can be divided into three temperature events. The first event is below 60 °C - its activity is lower than Ag-Sn/CeO_2 (3%) catalyst and presents 8% CO conversion at about 58 °C. The second temperature event is in the range of 60 to 120°C, where its activity is almost equal to Ag-Sn/CeO_2 (1%) catalyst. The third event is beyond 120 °C, where the slope again goes beneath the slope of Ag-Sn/CeO_2 (3%) catalyst. This irregular behavior of CeO_2 with temperature toward CO oxidation in comparison with other catalysts is due to the particle size, oxygen capturing property and thermal changes. At the same temperature, the four catalysts have exhibited relatively higher activities than the catalysts reported by Yu *et al.*[34] supplying the reaction mixture with flow rate of 50 cm^3 min^{-1}. This is because of silver loading with appropriate quantity and the incorporation of SnO in support platform for controlling the redox behavior of silver ion. The important factor that influences the activity of nanocatalysts is the particle size. The surface-to-volume ratio becomes larger and the concentration of partially coordinated surface sites becomes higher when the particle size decreases.[34] It has been usually observed by different researchers that the activity increases with decrease in particle size. In the present research work, there is a relationship between silver particle size and catalytic activity. Based on 99% CO conversion the activity of the four catalysts is in the order Ag-Sn/CeO_2 (4%) > Ag-Sn/CeO_2 (2%) > Ag-Sn/CeO_2 (1%) > Ag-Sn/CeO_2 (3%). In comparison, the particle size was also in the same order: Ag-Sn/CeO_2 (4%) > Ag-Sn/CeO_2 (2%) > Ag-Sn/CeO_2 (1%) > Ag-Sn/CeO_2 (3%), as illustrated from HRTEM and PXRD data (Table 1 and Figure 5). Particle size smaller than 3 nm is also the worst for Ag catalytic

activity because it leads to a wider band gap and results in metal to nonmetal transition owing to which it cannot dissociate molecular oxygen for the catalytic conversion of CO to CO_2. In the present studies, the particle size of Ag in Ag-Sn/CeO_2 (4%) catalyst is below 3 nm but presents superb catalytic activity among the other options. This behavior of the catalysts can be assigned to the electron donating effect of Sn (Electronegativity (E. N.) = 1.8 eV) for being less electronegative than Ag (E. N. = 1.9 eV), which results in shorter band gap and enhanced catalytic activity. In comparison to the work reported by Zhang *et al.*,[35,53] that Ag/SBA-0500 and Au/SiO2,catalysts have 98% CO conversion at 190 and 400 °C, respectively. El-Shall and co-workers[54-57] have reported the synthesis of Ag, Pd and Au (5 wt.%) nanoparticles and AuPd, PdAg (5 wt.%) bimetallic nanoalloys supported on CeO_2 for CO oxidation by two different methods, like laser vaporization and microwave irradiation. They found out that Pd/CeO_2 and Au/CeO_2nanocatalysts, developed by laser vaporization technique, have converted CO to CO_2 with 100% efficiency at 108 and 163 °C, respectively, while the catalyst combinations Ag/CeO_2, Pd/CeO_2 and Au/CeO_2 synthesized via microwave irradiation showed 100% CO to CO_2 conversion at 266, 151, and 301 °C, respectively (Table 2). The bimetallic nanoalloys, supported on CeO_2 and synthesized by microwave irradiation, have demonstrated 93% CO conversion at 186 °C. The catalyst combination Ag-Sn/CeO_2 (4%), presented in this study, has demonstrated 100% CO to CO_2 conversion at 100 °C, which is the superb catalytic activity among the other options. This excellent catalytic performance could be attributed to the strong metal-support electronic interaction, which controls the redox behavior of silver nanoparticles.

To evaluate the long term stability and reproducibility of the designed nanocatalysts stability, tests were performed under stationary condition and fixed temperature. The

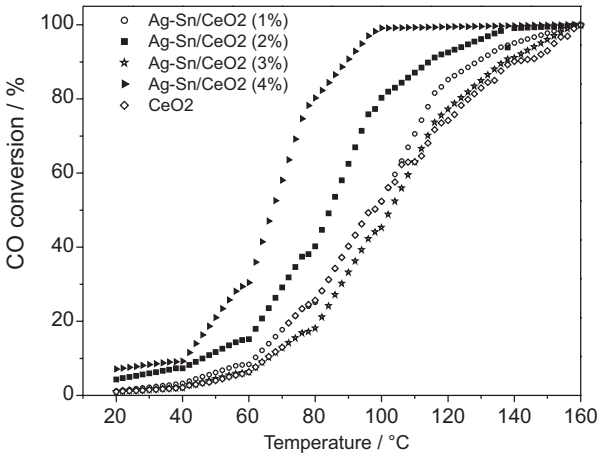

Figure 8. Catalytic activity for CO oxidation of Ag-Sn/CeO_2 catalysts with different Ag-Sn wt.% loading and CeO_2 support. The reactor effluent was analyzed using an online gas chromatograph system with Molecular Sieves 5A (30 m) column and TCD detector.

stability of CeO_2 supported nanocatalysts was tested for 900 min (15 h) at 110 °C and the results are shown in Figure 9. In the selected time period, the stability of the catalysts is in the order: Ag-Sn/CeO_2 (4%) > Ag-Sn/CeO_2 (3%) > Ag-Sn/CeO_2 (2%) > Ag-Sn/CeO_2 (1%) = CeO_2. Surprisingly, the CO conversion over the 4, 2 and 3% catalysts is as high as 97, 85 and 64%, respectively, for about 700 min. These values decrease slowly to 95, 80 and 60% after keeping the catalysts at 110 °C for 900 min. The 4, 2 and 3% catalysts have demonstrated 5, 8 and 6% stability loss in the whole testing period, respectively. Possible explanation for the long term stability of these catalysts is the appropriate quantity of metal loading on support and their mutual interaction for reproducing their electronic states, which is a key factor for catalytic recycling. The behavior of Ag-Sn/CeO_2 (1%) catalyst is different from the other options and the CO conversion percentage decreases from 79 to 40% with 39% stability loss for 900 min at

Table 2. CO oxidation over Ag-Sn/CeO_2 catalysts with different Ag-Sn wt.% loading and literature reported catalytic activities of Pd, Au, Ag nanoparticles and AuPd, PdAg bimetallic nanoalloys supported on CeO_2

Sample	C_{co} (60 °C)[a] / %	T_{30} (CO)[b] / °C	T_{99} (CO)[b] / °C	Reference
Ag-Sn/CeO_2 (1%)	09	84	152	This work
Ag-Sn/CeO_2 (2%)	16	73	133	This work
Ag-Sn/CeO_2 (3%)	07	90	157	This work
Ag-Sn/CeO_2 (4%)	36	59	98	This work
Pd/CeO_2 (5%)	–	–	108	54,55
Au/CeO_2 (5%)	–	–	163	54,55
Pd/CeO_2 (5%)	–	–	151	56
Au/CeO_2 (5%) SP[c]	–	–	301	56
Ag/CeO_2 (5%)	–	–	266	57
AuPd/CeO_2 (5%)	–	–	186(93%)	57
PdAg/CeO_2 (5%)	–	–	174(94%)	57

[a]Percent conversion of CO at 60 °C; [b]temperatures for 30 and 99% conversion; [c]separately precipitated.

110 °C. Similar behavior to Ag-Sn/CeO_2 (1%) catalyst for pure CeO_2 support was observed under the same testing conditions.

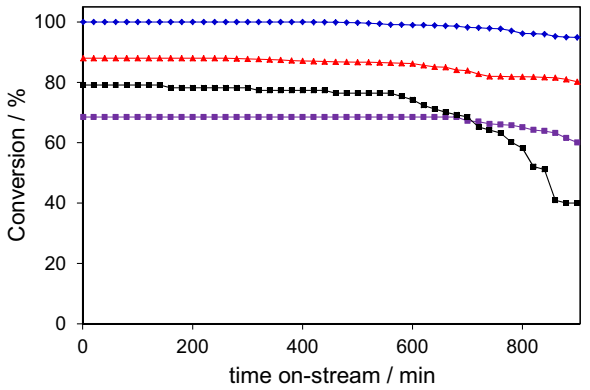

Figure 9. Stability performance of the nanocatalysts supported on CeO_2: (a) 4%; (b) 2%; (c) 3%; and (d) 1%. Testing condition: 1 vol.% CO, 2 vol.% O_2 and Ar balanced, 110 °C, 35 cm^3 min^{-1}.

Conclusions

In summary, catalyst combinations like Ag-Sn/CeO_2 with different Ag-Sn wt.% loading were synthesized by co-precipitation method, characterized by a range of instrumental techniques and tested for catalytic CO oxidation reaction. PXRD and HRTEM analyses confirmed that these catalysts have small particles with narrow size distribution over support surface. UV-Vis and H_2-TPR measurements have recommended strong metal-support interaction, which expedites the catalytic activity and catalysts stability. The catalysts are classified by increasing the order of their activity as Ag-Sn/CeO_2 (3%) < Ag-Sn/CeO_2 (1%) < Ag-Sn/CeO_2 (2%) < Ag-Sn/CeO_2 (4%) after their testing for CO oxidation reaction. The Ag-Sn/CeO_2 (4%) catalyst is the most promising catalyst combination of this study among the other options, which presents 100% CO oxidation at 100 °C and only 5% stability loss at 110 °C for 900 min due to small particle size and strong metal-support interaction.

Acknowledgements

This work was supported by the Higher Education Commission (HEC) of Pakistan (No. 20-1638/R&D/09/2900). The authors thank PhD Dalaver Hussain Anjum (KAUST Saudi Arabia) for high resolution TEM and SAED analyses.

References

1. Dai, W. L.; Yong, C.; Ren, L. P.; Yang, X. L.; Xu, J. H.; Li, H. X.; He, H. Y.; Fan, K. N.; *J. Catal.* **2004**, *228*, 80.
2. Shi, C.; Cheng, M. J.; Qu, Z. P.; Bao, X. H.; *J. Mol. Catal. A: Chem.* **2005**, *235*, 35.
3. Lee, J. H.; Schmieg, S. J.; Oh, S. H.; *Appl. Catal., A* **2008**, *342*, 78.
4. van Santen, R. A.; Kuipers, H. P. C. E.; *Adv. Catal.* **1987**, *35*, 265.
5. Zhang, L.; Zhang, C. B.; He, H.; *J. Catal.* **2009**, *261*, 101.
6. Nagy, A. J.; Mestl, G.; Schlögl, R.; *J. Catal.* **1999**, *188*, 58.
7. Yamamoto, R.; Sawayama, Y.; Shibahara, H.; Ichihashi, Y.; Nishiyama, S.; Tsuruya, S.; *J. Catal.* **2005**, *234*, 308.
8. Purcar, V.; Donescu, D.; Petcu, C.; Luque, R.; Macquarrie, D. J.; *Appl. Catal., A* **2009**, *363*, 122.
9. Magaev, O. V.; Knyazev, A. S.; Vodyankina, O. V.; Dorofeeva, N. V.; Salanov, A. N.; Boronin, A. I.; *Appl. Catal., A* **2008**, *344*, 142.
10. Frey, K.; Iablokov, V.; Melaet, G.; Guczi, L.; Kruse, N.; *Catal. Lett.* **2008**, *124*, 74.
11. Song, K. S.; Kang, S.; Sim, S. D.; *Catal. Lett.* **1997**, *49*, 65.
12. Xu, R.; Wang, X.; Wang, D. S.; Zhou, K. B.; Li, Y. D.; *J. Catal.* **2006**, *237*, 426.
13. Wang, A. Q.; Liu, J. H.; Lim, S. D.; Lin, T. S.; Mou, C. Y.; *J. Catal.* **2005**, *233*, 186.
14. Wang, A. Q.; Hsieh, Y. P.; Chen, Y. F.; Mou, C. Y.; *J. Catal.* **2006**, *237*, 197.
15. Liu, X. Y.; Wang, A. Q.; Yang, X. F.; Zhang, T.; Mou, C. Y.; Su, D. S.; Li, J.; *Chem. Mater.* **2009**, *21*, 410.
16. Liu, H. Y.; Ma, D.; Blackley, R. A.; Zhou, W. Z.; Bao, X. H.; *Chem. Commun.* **2008**, *23*, 2677.
17. Zhang, X.; Qu, Z.; Li, X.; Wen, M.; Quan, X.; Ma, D.; Wu, J.; *Sep. Purif. Technol.* **2010**, *72*, 395.
18. Bao, X.; Muhler, M.; Pettinger, B.; Schlögl, R.; Ertl, G.; *Catal. Lett.* **1993**, *22*, 215.
19. Bao, X.; Muhler, M.; Pettinger, B.; Schlögl, R.; Ertl, G.; *Catal. Lett.* **1995**, *32*, 185.
20. Schubert, H.; Tegtmeyer, U.; Herein, D.; Bao, X.; Muhler, M.; Schlögl, R.; *Catal. Lett.* **1995**, *33*, 305.
21. Su, D. S.; Jacob, T.; Hansen, T. W.; Wang, D.; Schlögl, R.; Freitag, B.; Kujawa, S.; *Angew. Chem., Int. Ed.* **2008**, *47*, 5005.
22. Qu, Z. P.; Cheng, M. J.; Huang, W. X.; Bao, X. H.; *J. Catal.* **2005**, *229*, 446.
23. Christopher, J. B.; Charles, A. M.; *J. Catal.* **1999**, *184*, 224.
24. Gardner, S. D.; Hoflund, G. B.; Upchurch, B. T.; Schryer, D. R.; Kielin, E. J.; Schryer, J.; *J. Catal.* **1991**, *129*, 114.
25. Gardner, S.; Hoflund, G.; Schryer, D.; Schryer, J.; Upchurch, B.; Kielin, E.; *Langmuir* **1991**, *7*, 2135.
26. Qu, Z.; Cheng, M.; Huang, W.; Bao, X.; *J. Catal.* **2005**, *229*, 446.
27. Pietron, J.; Stroud, R.; Rolison, D.; *Nano Lett.* **2002**, *2*, 545.
28. Qu, Z. P.; Huang, W. X.; Cheng, M. J.; Bao, X. H.; *J. Phys. Chem. B* **2005**, *109*, 15842.

29. Bamwenda, G.; Tsubota, S.; Nakamura, T.; Haruta, M.; *Catal. Lett.* **1997**, *44*, 83.
30. Hu, R. R.; Xie, L. Y.; Ding, S.; Hou, J.; Cheng, Y.; Wang, D. Z.; *Catal. Today* **2008**, *131*, 513.
31. Comsup, N.; Panpranot, J.; Praserthdam, P.; *Catal. Commun.* **2010**, *11*, 1238.
32. Dai, Y. M.; Pan, T. C.; Liu, W. J.; Jehng, J. M.; *Appl. Catal., B* **2010**, *103*, 221.
33. Afanasev, D. S.; Yakovina, O. A.; Kuznetsova, N. I.; Lisitsyn, A. S.; *Catal. Commun.* **2012**, *22*, 43.
34. Yu, L. B.; Shi, Y. Y.; Zhao, Z.; Yin, H. B.; Wei, Y. C.; Liu, J.; Kang, W. B.; Jing, T. S.; Wang, A. L.; *Catal. Commun.* **2011**, *12*, 616.
35. Zhang, X.; Qu, Z.; Yu, F.; Wang, Y.; *J. Catal.* **2013**, *297*, 264.
36. Zhu, H. G.; Liang, C. D.; Yan, W. F.; Overbury, S. H.; Dai, S.; *J. Phys. Chem. B* **2006**, *110*, 10842.
37. Sun, J. M.; Ma, D.; Zhang, H.; Liu, X. M.; Han, X. W.; Bao, X. H.; Weinberg, G.; Pfänder, N.; Su, D. S.; *J. Am. Chem. Soc.* **2006**, *128*, 15756.
38. Backx, C.; de Groot, C. P. M.; Biloen, P.; *Surf. Sci.* **1981**, *104*, 300.
39. Wei, T. C.; Phillips, J.; *Adv. Catal.* **1996**, 41, 359.
40. Bao, X.; Barth, J. V.; Lehmpfuhl, G.; Schuster, R.; Uchida, Y.; Schlögl, R.; Ertl, G.; *Surf. Sci.* **1993**, *284*, 14.
41. Marta, C. N.; de Carvalho, A.; Passos, F. B.; Schmal, M.; *J. Catal.* **2007**, *248*, 124.
42. Bron, M.; Teschner, D.; Wild, U.; Steinhauer, B.; Knop-Gericke, A.; Volckmar, C.; Wootsch, A.; Schlögl, R.; Claus, P.; *Appl. Catal., A* **2008**, *341*, 127.
43. Shimizu, K.; Miyamoto, Y.; Satsuma, A.; *ChemCatChem* **2010**, *2*, 84.
44. Li, K.; Wang, Y.; Wang, S.; Zhu, B.; Zhang, S.; Huang, W.; Wu, S.; *J. Nat. Gas Chem.* **2009**, *18*, 1.
45. Avgouropoulos, G.; Ioannides, T.; *Appl. Catal., A* **2003**, *244*, 155.
46. Chen, Y.; Zhang, L. F.; *Catal. Lett.* **1992**, *12*, 51.
47. Djuričić, B.; Pickering, S.; *J. Eur. Ceram. Soc.* **1999**, *19*, 1925.
48. Bensalem, A.; Bozon-Verduraz, F.; Delamar, M.; Bugli, G.; *Appl. Catal., A* **1995**, *121*, 81.
49. Kharlamova, T.; Mamontov, G.; Salaev, M.; Zaikovskii, V.; Popova, G.; Sobolev, V.; Knyazev, A.; Vodyankina, O.; *Appl. Catal., A* **2013**, *467*, 519.
50. Yen, H.; Seo, Y.; Kaliaguine, S.; Kleitz, F.; *Angew. Chem., Int. Ed.* **2012**, *51*, 12031.
51. Yatsimirskii, V. K.; Oleksenko, L. P.; Lutsenko, L. V.; Chen, Y.; *Russ. J. Phys. Chem. A* **2008**, *82*, 1460.
52. Giordano, F.; Trovarelli, A.; Leitenburg, C.; Giona, M.; *J. Catal.* **2000**, *193*, 273.
53. Qian, K.; Jiang, Z. Q.; Huang, W. X.; *J. Mol. Catal. A: Chem.* **2006**, *264*, 26.
54. Yang, Y.; Saoud, K. M.; Abdelsayed, V.; Glaspell, G.; Deevi, S.; El-Shall, M. S.; *Catal. Commun.* **2006**, *7*, 281.
55. Glaspell, G.; Hassan, H. M. A.; Elzatahry, A.; Abdalsayed, V.; El-Shall, M. S.; *Top. Catal.* **2008**, *47*, 22.
56. Glaspell, G.; Fuoco, L.; El-Shall, M. S.; *J. Phys. Chem. B* **2005**, *109*, 17350.
57. Abdalsayed, V.; Aljarash, A.; El-Shall, M. S.; Al Othman, Z. A.; Alghamdi, A. H.; *Chem. Mater.* **2009**, *21*, 2825.

Submitted: May 31, 2014
Published online: February 6, 2015